www.amlett.com, www.amlett.org, DOI: 10.5185/amlett.2013.2417 Published online by the VBRI press in 2013

Experimental finding of initiation fracture toughness and FEM simulation of fracture behaviour of UFG 7075 Al alloy

Prosenjit Das[1*], R. Jayaganthan[2], I. V. Singh[3]

[1]Foundry Group, CSIR-Central Mechanical Engg. Research Institute (CSIR-CMERI), Durgapur 713209, India
[2]Department of Metallurgical and Materials Engineering & Centre of Nanotechnology, Indian Institute of Technology Roorkee, Roorkee 247667, India
[3]Department of Mechanical and Industrial Engineering, Indian Institute of Technology Roorkee, Roorkee, 247667, India

*Corresponding author. Tel: (+91) 343 6452373; Fax: (+91) 343 2546745; E-mail: prosenjit@cmeri.res.in

Received: 04 February 2013, Revised: 18 April 2013 and Accepted: 01 May 2013

ABSTRACT

The present work describes an experimental evaluation of yield strength, tensile strength, initiation fracture toughness and Finite element simulations of fracture behaviour for both bulk and ultrafine-grained (UFG) 7075 Al Alloy. The 7075 Al alloy has been rolled for different thickness reductions (40%, 70% and 90%) at cryogenic (liquid nitrogen) temperature, and its mechanical properties and microstructural morphology have been investigated. Rolling of the Al alloy at cryogenic temperature suppresses the dynamic recovery and grain growth, which leads to grain fragmentation. Dislocation cells formed during consecutive rolling passes, transformed into fully formed UFG (600 nm) up to 70% thickness reduction. Grain size gets reduced further when 90% thickness reduction is achieved. Incremental crack growth simulations have been carried out by commercial software ABAQUS under quasi-static loading using deformation plasticity theory based on Griffith energy concept. *J*-integral, stress along crack path, effect of crack and specimen size over *J*-integral, stress distribution and plastic dissipation ahead of the crack tip have been investigated for some practical crack problems under mechanical and thermo-mechanical loading. The numerical examples indicates a significant enhancement in crack arrest capabilities of UFG alloys for the same boundary conditions because of decreasing *J* values with increasing % thickness reduction. This is attributed to the improved mechanical properties (UTS: 625 MPa and YS: 610 MPa) of the cryorolled alloy which hinders the onset of plasticity, results from ultrafine-grain formation.

Keywords: Aluminum; UFG alloy; cryorolling; mechanical testing; fracture toughness; FEM.

Prosenjit Das is presently working as a Scientist with Foundry group at CSIR-Central Mechanical Engineering Research Institute, India. His areas of research are advanced materials and manufacturing processes, Mechanics of Materials, Computational Material Science, Casting & Solidification etc. He has written 45 scientific papers till date in different international journals and international/national conferences. He has done his graduation from Kalyani Govt. Engg. College, India and post graduation from Indian Institute of Technology Roorkee, India.

R. Jayaganthan has done PhD in Materials Engg from IISC Bangalore, India and currently is an Associate Professor at the Dept of Metallurgical and Materials Engg & Centre of Naotechnology of Indian Institute of Technology Roorkee. His area of research is Nano materials and has written over 100 scientific papers.

I. V. Singh is an Associate Professor at the Dept of Mechanical and Industrial Engg. of Indian Institute Of Technology Roorkee. He mainly works in the area of computational fracture mechanics. He performs the modeling and simulations of fracture and fatigue behavior of materials. He is also developing constitutive models for Al-alloys. He has written over 100 scientific papers till date.

Introduction

Ultrafine-grained materials are the subject of focus in the arena of materials research to realize its potential for structural and functional applications, in recent years. Various severe plastic deformation (SPD) processes like equal channel angular pressing (ECAP), multiple compressions, equal channel angular extrusion (ECAE) and severe torsional straining used for the production of fully dense ultrafine grained and nanostructured materials from their bulk counterparts materials without the introduction of any contaminants. The formation of ultrafine grain structures by SPD methods, provides very large deformations at relatively low temperatures and under high pressures **[1-2]**. Present work describes the production of ultrafine-grained 7075 Al alloy using cryorolling technique (rolling at liquid nitrogen temperature). Rolling at cryogenic temperature suppresses dynamic recovery, grain growth and the fragmented dislocation cells reaches to a higher steady state level as compared to the room temperature rolling. With consecutive cryo-rolling passes, these dense dislocation cells are converted into grain fragments or ultrafine grain structures (UFG) with high angle grain boundaries. Earlier literature also reports about the improved tensile, hardness properties of pure Cu, Ni, Al and their alloys due to formation of UFG by SPD **[3-7]**.

7075 aluminum alloy is widely used in aircraft structures due to their excellent mechanical properties such as low density, high strength, ductility, toughness, resistance to fatigue and high strength to weight ratio **[1-4]**. Till date, there is not much available literature on mechanical and fracture behavior of UFG 7075 Al-alloy **[8, 9]**. Therefore, first tensile, hardness and initiation fracture toughness properties of both bulk and UFG Al alloys are evaluated experimentally and then the incremental crack growth simulations have been performed, using finite element method (FEM). To investigate the possible improvement in fracture behavior of cryorolled alloy due to ultrafine nanoscale grain formation **[10]** compared to its bulk form, the fracture mechanics simulations are performed in commercial software ABAQUS since experiments are expensive, difficult, and time consuming. FEM has been opted as numerical tool to simulate the fracture mechanics problems due to its competency and accuracy. In general, Al-alloys are ductile in nature; hence elastic-plastic fracture simulations of both bulk and UFG Al alloy are carried out under quasi-static mode-I loading using the deformation plasticity theory **[11-15]**.

Section 2.0 describes the experimental procedure for evaluating the mechanical properties whereas section 3.2 presents an experimental evaluation of the mechanical properties of cryorolled Al alloys. A brief description of *J*-integral which has been used as the failure criterion and measure of fracture toughness in small scale yielding conditions is given in section 3.6.

The present study is aimed to investigate the crack arrest capabilities of cryorolled 7075 Al alloy. Previous work performed by this group **[7-9, 15-17]** establishes UFG form of the alloy as a potential candidate to replace the bulk form in case of aerospace structural applications. Being a potential alloy for possible aerospace appliances, fracture behaviour and crack arrest capabilities of the said alloy is of outmost importance. Efforts have been made in this study to apply an incremental crack growth simulation technique to investigate the crack healing ability of the UFG alloy. Effect of alloying elements on fracture behaviour is also investigated in detail within the scope of the present work.

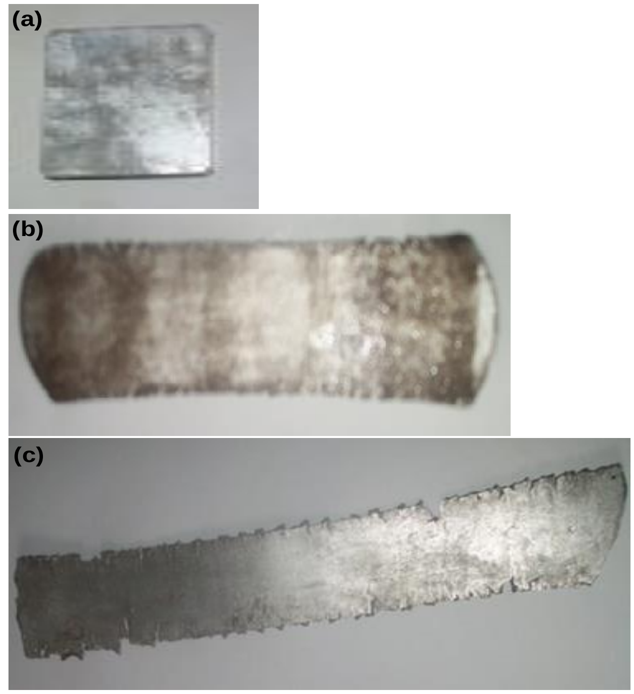

Fig. 1. Photograph of the samples: (a) before cryorolling, (b) 70% cryorolled and (c) 90% cryorolled.

Experimental

Materials

The 7075 Al alloy has been procured from Hindustan Aeronautics Ltd., Bangalore, India in the form of extruded ingot with 50 mm diameter, for the present work. Chemical composition of the alloy used in the work is 6.04% Zn, 3.64% Mg, 1.76% Cu, 0.50% Cr, 0.2% Si, 0.15% Mn, 0.57% Fe, and Al balance (weight percentage).

Cryorolling of 7075 Al alloy

The as received Al ingot has been machined into small plates and then solution treated (ST) at 490 ^{0}C for 6 hours, followed by quenching treatment in water at room temperature **[8,9,16]** to homogenize the microstructure. Solution treatment also aids to dissolve the precipitates in the solid-solution, prior to cryorolling at liquid nitrogen temperature. The Al alloy plates after solution treatment (ST) are subjected to cryorolling (rolling at liquid nitrogen atmosphere) and room temperature rolling to achieve 40%, 70% and 90% thickness reductions. Prior to each roll pass, samples have been dipped in liquid nitrogen for 30 minutes for the effective suppression of recovery, so as to accumulate dislocation density during rolling at liquid nitrogen temperature.

The diameter of rolls and rolling speed are 110 mm and 8 rpm, respectively. The temperature of the samples have been measured, before and after cryorolling. The temperatures are: 190 ^{0}C and -150 ^{0}C, respectively, in each pass. To prevent temperature rise of the samples, after cryorolling (CR), samples have been put back immediately into the cryocan, within 40-50 seconds. $MoSi_2$ has been used as solid lubricant during the rolling process to minimize the frictional heat. Maximum achievable reduction per rolling pass is 5%, but many passes are given to achieve uniform grain structure throughout cross-section of the samples. **Fig. 1** shows the photograph of the solution treated and cryorolled samples so that the reader can see the morphology change occurred within the material due to cryorolling.

Micro hardness and tensile tests have been performed for starting bulk Al alloy and UFG Al alloy (Cryorolled and room temperature rolled), subjected to various strains. Vickers macro hardness (H_V) has been measured on the top plane of the sample, parallel to longitudinal axis (rolling direction), by applying a load of 15 kg for 15 s. The surface of the specimen is polished mechanically using emery paper prior to each H_V measurement to ensure its clean surface. As per the standards, the samples are polished to get a smooth and shiny surface before the hardness test. The hardness value taken is an average of ten measurements made on surface of each specimen. The tensile specimens have been prepared in accordance with American Society for Testing and Materials (ASTM) Standard E-8/E8M-09 **[18]** sub-size specifications parallel to the rolling direction with a 25 mm. gauge length. The tensile test is performed after polishing the samples in air at room temperature using an S series, H25K-S materials testing machine, operated at a constant crosshead speed and with an initial strain rate of 5×10^{-4} s^{-1}. Tensile samples have been polished before the testing to remove all the scratches and tiny cracks. The samples with different percentage of thickness reduction, after cryorolling, have been machined to the same length, without changing the thickness for tensile test. The tensile results considered in the present work are an average of three measurements, for each testing condition.

Fracture behaviour of 7075 Al alloy was investigated using compact tension specimens. The geometry of the compact tension [C(T)] specimen is shown in our previously published work **[9]**. The specimens tested for cryorolled (CR) conditions have been e machined from the rolled plate with their tensile axis parallel to the rolling direction. All specimens are fatigue precracked for a crack length/width (a/w) ratio of 0.5 following the ASTM standard E647-08 **[19]**. The pre-cracking has been carried out on a computer controlled servo hydraulic Instron machine (model 8502). All pre-cracking are made at a stress ratio of R = 0.1 at 10 Hz frequency, employing decreasing stress intensity factor range (ΔK) envelope. The final ΔK at the end of pre-cracking is maintained between 12 and 15 MPa $\sqrt{m}$. The crack length during pre-cracking is monitored using travelling microscope to reach a predetermined length marking. Plain strain fracture toughness tests have been carried out, as per the guidelines of ASTM standard E 1820-08a **[20]** on a 50 kN servo-hydraulic Instron machine (model 8502) at a displacement rate of 0.003 mm/s at laboratory ambient temperature (27^0C). The loading sequence applied for monotonic fracture test is shown in **Fig. 2.** A clip gauge with a travel of 5 mm is used during the fracture toughness tests to monitor the load line displacement (LLD). The load–LLD data for each of the specimen have been recorded for subsequent analysis to obtain the monotonic and cyclic J–R curves. The tests are stopped when the maximum load drops more than 20%. This criterion is selected to maintain uniformity in test completion for all fracture toughness tests in this investigation. After the completion of fracture tests, all specimens are post fatigue cracked, till separation, to mark the stable crack growth region.

Microstructural characterization of the bulk and UFG Al alloy has been carried out by using Field emission scanning electron microscopy (FE-SEM) and fracture surfaces of C.T specimens are examined with the help of a Scanning electron microscope (SEM) (model: HITACHI, N-3000).

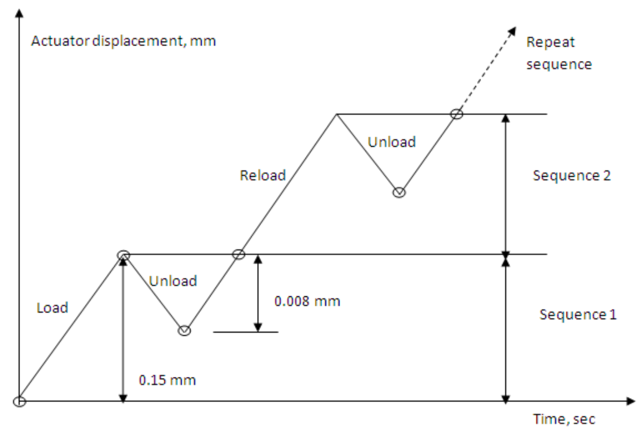

Fig. 2. Loading sequence of fracture toughness tests.

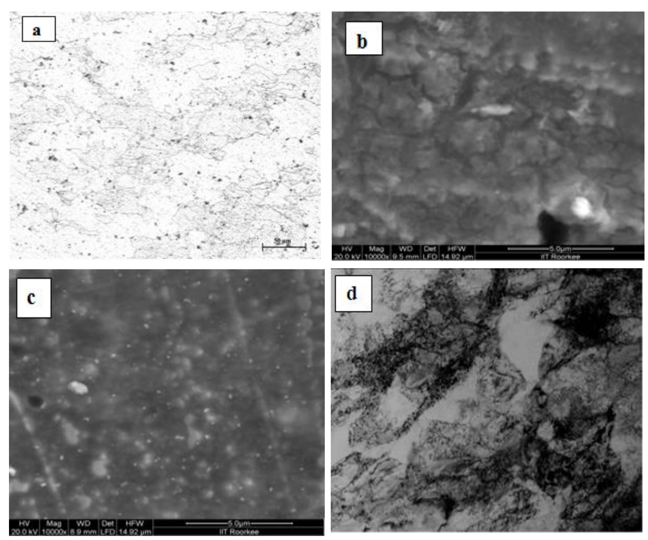

Fig. 3. (a) Optical micrograph of starting material, FESEM image of (b) 40 CR and (c) 70 CR and Transmission electron micrograph of (d) 90 CR **[3]**.

Results and discussion

Microstructure characterization

Microstructure characterization of the starting bulk 7075 Al alloy is carried out by optical microscopy and SEM micrographs are taken to characterize the cryorolled (UFG) Al alloys. In this context it should be mentioned that the rolling of the said alloy at cryogenic temperature leads to the suppression of dynamic recovery and dislocation accumulation. With the multiple cryorolling (CR) passes, these accumulated dislocations finally facilitates ultrafine grain formation (ufg) undergoing sub-structuring in between.

Micrographs of bulk and UFG Al alloys, after 40%, 70% and 90% thickness reduction, are shown in **Fig. 3** (a-d). The samples are cut from longitudinal (rolling) direction for microstructural characterization. The microstructure of bulk Al alloy exhibits lamellar grains lying parallel to the ingot axis. The average grain size is around 40μm. The grain size is reduced to around 950 nm for the CR samples subjected to 40% thickness reduction and fully formed ultrafine-grains (around 600 nm) are observed after 70% thickness reduction, as seen from the **Fig. 3** (b & c). Whereas, nearly 26 µm and 10 µm are the grain sizes observed in case of RTR samples subjected to 40% and 70% thickness reductions, respectively. The grain sizes are higher in case of RTR alloy, due to much lower dislocation density. Further reduction in grain size is observed in case of 90% cryorolled samples, which is shown in **Fig. 3** (d) **[3]**. CR Al 7075 alloy shows high fraction of high angle grain boundaries and high amount of dislocation density as reported in our earlier work **[3, 8, 9,16]**.

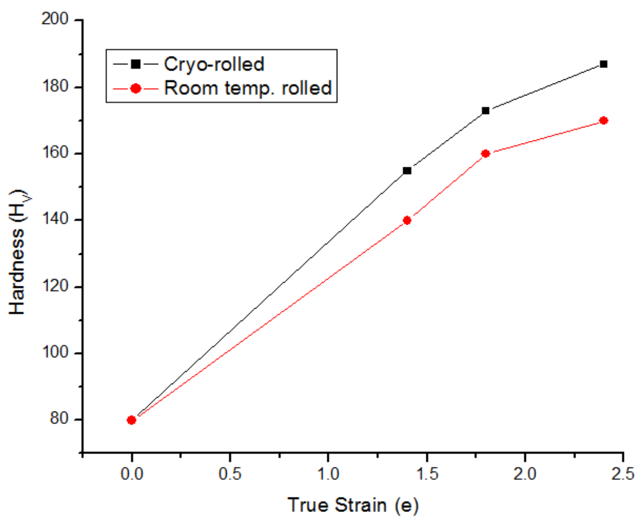

Fig. 4. Vickers hardness properties of cryorolled and room temp rolled materials as a function of total amount of deformation.

Mechanical properties

A significant improvement in mechanical properties achieved is due to the ultrafine-grain formation, facilitated by cryorolling process. **Fig. 4** shows the Vickers hardness values of the starting bulk 7075 Al alloy and its solution treated form, which has been rolled at cryogenic temperature and room temperature (RT), respectively as a function of true rolling strain. The true strain corresponds to different percentage of thickness reduction in the samples. The relation between true strain and thickness reduction percentage is shown below,

$$Truestarin = \ln\{\frac{FinalThickness(T_f)}{InitialThickness(T_i)}\} \qquad (1)$$

The hardness of the cryorolled materials has increased from 80 to 155 H_v (nearly 94% increase) after 40 percent thickness reduction (e = 1.4) and after 70 percent thickness reduction (e = 1.8) it increases to 173 H_v (nearly 117% increase). Subsequent thickness reductions of the samples increased its hardness further and after 90 percent thickness reduction (e=2.4), it has increased about 134%. It is observed that the hardness of CR alloys is higher than that of room tempearture rolled (RTR) materials at different strains, due to increased dislocation density and the formation of ultra fine grains in the CR alloys.

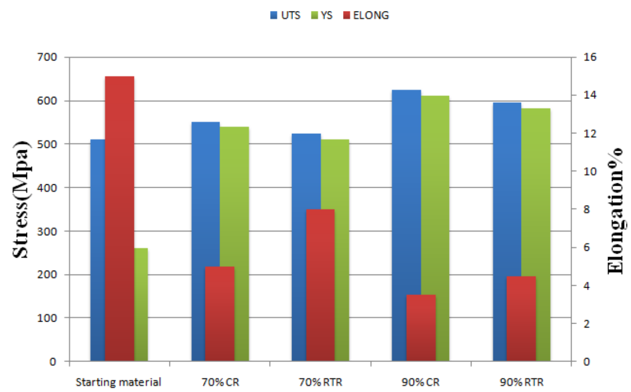

Fig. 5. Tensile properties of Al 7075 alloy after different percentage of thickness reduction: (1) Starting, Bulk alloy, (2) CR at 40% reduction, (3) RTR at 40% reduction, (4) CR at 70% reduction, (5) RTR at 70% reduction, (6) CR at 90% reduction and (7) RTR at 90% reduction.

Fig. 5 shows the tensile properties of Al 7075 alloy CR and RTR at different percentage of thickness reductions (40%, 70% and 90%). It is observed that the tensile strength (UTS) of CR samples has increased from 500 MPa to 530 MPa (nearly 6% increase), whereas yield strength (YS) has increased from 260 MPa to 430 MPa (nearly 66% increase) for 40% thickness reduction (*e* = 1.4). The observed tensile and yield strength for the 40% thickness reduced RTR samples were 515 MPa and 395 MPa, respectively. Similarly, for the CR samples with 70% thickness reduction (*e* = 1.8), UTS has increased from 500 MPa to 550 MPa (nearly 10% increase) and YS has increased from 260 MPa to 540 MPa (nearly 108% increase), whereas tensile and yield strength for the 70% thickness reduced RTR samples were 525 MPa and 510 MPa, respectively. For the CR samples with 90% thickness reduction (e=2.4), UTS and YS have increased to 625 MPa and 610 MPa respectively, as reported in our earlier work **[3]**. Tensile strength of CR alloys are found higher than that of the starting bulk alloy and RTR alloys, due to the higher amount of dislocation density and sub-grain formation in the CR alloys. The influence of cryorolling treatment on yield strength (YS) is substantial as compared to that of it on ultimate tensile strength of the cryorolled samples, due to effective grain refinement. The alloying elements such as Zn and Mg, present in the said alloy, tends to form precipitates. The precipitates are useful for increasing the hardness and tensile properties of Al 7075 alloy. Tensile test results of 90% cryorolled samples are compared with 40 and 70% reduced samples, which are used further for FEM analysis in the present work.

7075 Aluminum alloy is used in aircraft structures due to their excellent mechanical properties such as low density, high strength, ductility, toughness, resistance to fatigue and high strength to weight ratio. Cryorolled form (UFG) of the abovementioned alloy is a potential candidate for possible aerospace appliances because of its significantly improved mechanical properties, fracture behaviour and crack arrest capabilities, as evident from the present study. Comparison of mechanical properties of different aerospace grade Al alloys are listed in **Table 1**.

Table 1. Comparison of mechanical properties of different aerospace grade Al alloys.

Aerospace Al alloys and processing routes	Ultimate tensile strength (UTS) in MPa	Yield strength (YS) in MPa	% Elongation
6063-T6 tempered	196	165	8
6061-T6 tempered	300	241	8-10
2024-T3 tempered	400-427	269-276	10-13
7075-T6 tempered	510-572	434-503	10-11
90% thickness reduced UFG-7075	625	610	14

J-R curve determination

For fracture toughness testing, samples are cut from longitudinal (rolling) direction. The compact tension specimens have been prepared as per the ASTM Standard E 1820-08a [20]. Crack length in monotonic J (Effective energy release rate)–R (Crack resistance) tests, is calculated from the linear portion of the unloading curve as shown in Fig 2. The relevant equations are shown below.

$$a_i/W = [1.000196 - 4.06319u + 11.242u^2 - 106.043u^3 + 464.335u^4 - 650.677u^5] \quad (2)$$

where, a_i/W = ratio of current crack size (crack size at i^{th} point) and specimen width.

$$u = \frac{1}{[B_e E C_{c(i)}]^{1/2} + 1} \quad (3)$$

$C_{c(i)}$ = specimen load-line crack opening elastic compliance $(\Delta v / \Delta P)$ on an unloading/reloading sequence corrected for rotation.

$$B_e = B - (B - B_N)^2 / B \quad (4)$$

The crack size is corrected to account for rotation as follows:

$$C_{c(i)} = \frac{C_i}{[\frac{H}{R}\sin\theta_i - \cos\theta_i][\frac{D}{R}\sin\theta_i - \cos\theta_i]} \quad (5)$$

where, C_i = measured specimen elastic compliance (at the load line), calculated from the least square fitting of linear portion of the unloading load-load line displacement curve. H = initial half-span of the load points (center of the pin holes), R = radius of rotation of the crack centerline, (W+a)/2, where a is the updated crack size, D = One half of the initial distance between the displacement measurement points, θ = angle of rotation of a rigid body element about the unbroken midsection line,

$$\theta = \sin^{-1}\left[\frac{(\frac{d_m}{2} + 2)}{(D^2 + R^2)^{1/2}}\right] - \tan^{-1}\left(\frac{D}{R}\right) \quad (6)$$

d_m = total measured load-line displacement. $(\Delta v / \Delta P)$ = differential crack opening displacement at notched edge/ differential load. σ_o = Yield stress of the material. B_e = Specimen thickness. B = Effective specimen thickness. B_N = net thickness (distance between root of the notch on both the specimen surfaces).

To validate the calculations, the calculated final crack length measured is compared with the physical crack length of the fracture method measured optically (Optical or SEM) by a 9 point average method (due to its thumbnail shape). The J values constitutes an elastic and a plastic part, which have been calculated as per ASTM Standard E 1820-08a **[20]**. After this calculation, the J versus Δa is plotted to get the J-crack resistance (R) curve **[21, 22]**. **Fig. 6** shows the Load-LLD plots and corresponding J-R curves for bulk and UFG (70% reduced) alloy which explains enhanced crack growth resistance of the cryorolled alloy due to ultrafine-grain formation.

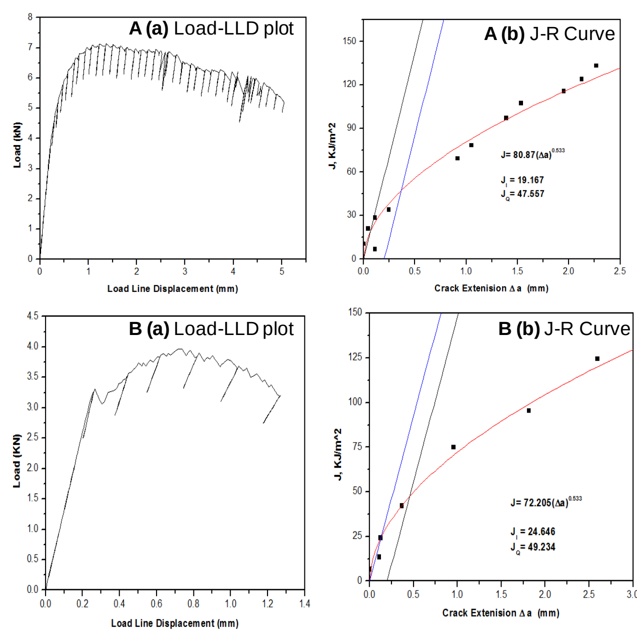

Fig. 6. Fracture parameters of (A) Starting bulk alloy, (B) 70% CR 7075 Al alloy.

Initiation fracture toughness (JI)

Increased fracture toughness observed in case of cryorolled samples is due to high density of dislocations, ultrafine-grain formation **[3,8,9,15,23]**, grain boundary sliding and increased fracture stress (σ_f) according to eq. (7) **[24]**.

$$\sigma_f = k_f\, d^{-1}, \tag{7}$$

where, k_f = Constant (MPa $m^{1/2}$), d= Grain size.

After plotting J versus Δa curve, a construction line determined, considering following eq^n:

$$J = M\ \sigma_y \Delta a \tag{8}$$

where, M=2, σ_y = materials yield strength, $\Delta a = a_i - a_{oq}$

a_{oq} = Revised a_i value considering determined J before specimen reached maximum force for the test. This revision procedure is as follows:

Identifying all J_I and a_i pairs, which are determined before the specimen reached the maximum force for the test and then using these data points a revised a_{oq} value has been calculated using the following equation:

$$a = a_{oq} + \frac{J}{2\sigma_0} + BJ^2 + CJ^3 \tag{9}$$

where, σ_o is the yield stress of the material. The coefficients (B and C) of the above equation has been calculated using a least squares fit procedure as per E1820 standard. Here, construction line cuts J versus Δa curve, that value is called the initiation fracture toughness (J_I) and where, 0.2 mm offset line (parallel to the construction line) cuts J versus Δa curve, gives the value of interim J_Q. Significant increase is found in J_I , which is increased from 19.167 KJ/m^2 (bulk alloy) to 24.646 KJ/m^2 (UFG-70% reduction). It explains improved crack arresting capabilities of the UFG alloy. J_Q has increased slightly from 47.557 KJ/m^2 (bulk alloy) to 49.234 KJ/m^2 (UFG-70% reduced).

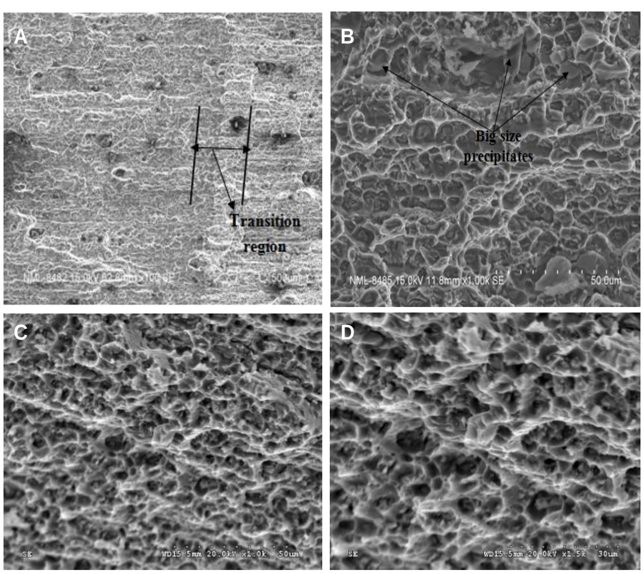

Fig. 7. SEM image of fracture surface of bulk alloy (A) Transition region (fatigue precrack and fracture), (B) Fracture surface, (C) Fracture surface, (D) Region-II at higher magnification.

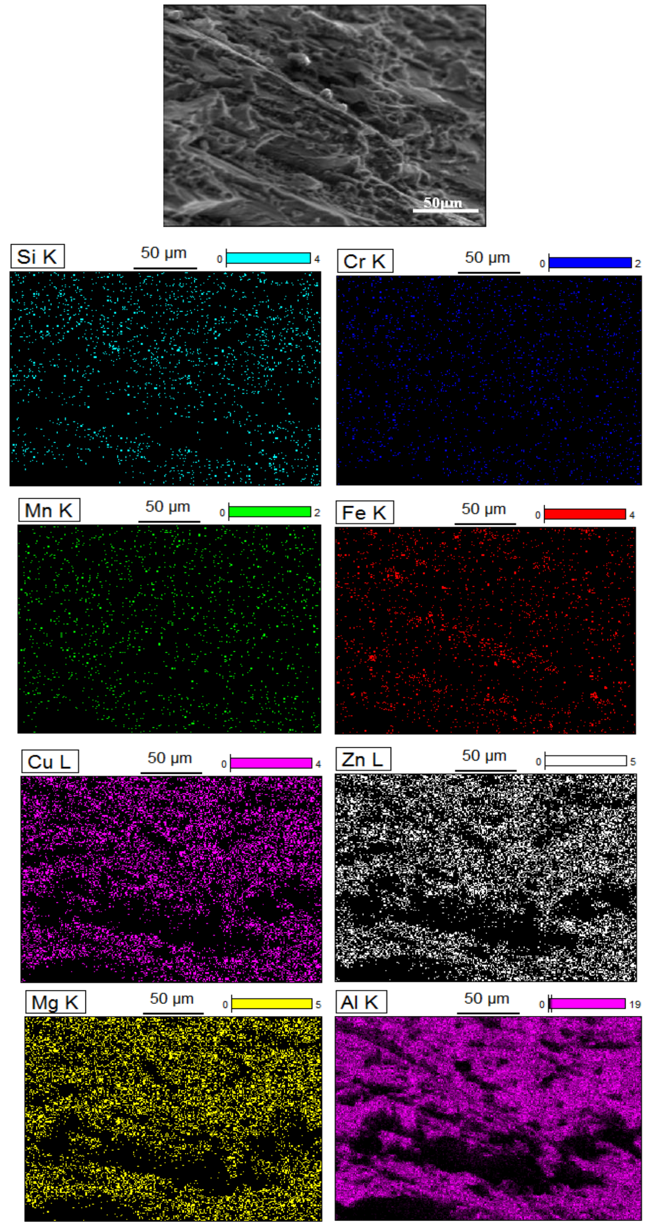

Fig. 8. X-ray mapping of the fracture surface of the bulk alloy.

Fracture surface morphology

SEM analysis of the fracture surfaces shows that the ductile fracture is the fracture mode for both UFG alloy and its bulk counterpart. Dimples are formed due to void growth and coalescence in the material at different processing conditions. Stretch zones are not observed distinctly from the fracture surfaces; however, transition region is clearly visible as shown in **Fig. 7**. Damage mechanism has transformed from striation governed smooth fatigue failure during precracking into void growth and coalescence driven ductile fracture under monotonic loading. It can be noted that the dimples are better formed in cryorolled (CR) alloy than in starting bulk alloy.

The precipitate formation tendency of alloying elements of the said alloy, such as Zn and Mg, effects the fracture toughness properties to some extent. Larger dimple size in case of starting bulk alloy (around 10 µm) is mainly caused by existence of inclusions and coarser precipitates

[25]. To analyze the effect of alloying elements on fracture properties and fracture surface morphology, detailed Scanning electron microscopy (SEM), X-ray mapping and spot analysis of the elements have been carried out at different regions over the fracture surface. The relevant results are shown in **Fig. 7, 8, 9**, respectively. Elemental compositions obtained from EDX plot, shown in Fig. 9a, are shown in **Table 2**.

Table 2. EDX composition results at region- I of the Bulk alloy fracture surface.

Element	Weight %	Weight % (Error)	Atom %	Atom %(Error)
Mg	3.01	+/- 0.06	3.66	+/- 0.07
Al	80.56	+/- 0.34	88.39	+/- 0.37
Si	0.66	+/- 0.09	0.69	+/- 0.09
Cr	0.23	+/- 0.06	0.13	+/- 0.03
Mn	0.04	+/- 0.08	0.02	+/- 0.04
Fe	0.42	+/- 0.09	0.22	+/- 0.05
Cu	3.79	+/- 0.34	1.76	+/- 0.16
Zn	11.31	+/- 0.51	5.12	+/- 0.23
Total	100.00		100.00	

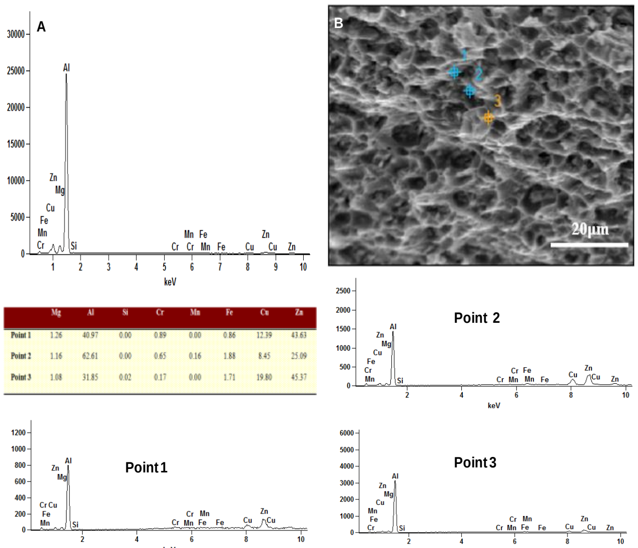

	Mg	Al	Si	Cr	Mn	Fe	Cu	Zn
Point 1	1.26	40.97	0.00	0.89	0.00	0.86	12.39	43.63
Point 2	1.16	62.61	0.00	0.65	0.16	1.88	8.45	25.09
Point 3	1.08	31.85	0.02	0.17	0.00	1.71	19.80	45.37

Fig. 9. (A) EDX results at fracture surface of the Bulk 7075 Al alloy (region I of Fig. 7) and **(B)** Point analysis (at three different points) over the fracture surface of the bulk alloy.

Table 3. EDX composition results at region- I of the UFG alloy fracture surface.

	Weight %	Weight % (Error)	Atom %	Atom %(Error)
Mg	3.54	+/- 0.08	4.21	+/- 0.10
Al	83.83	+/- 0.33	89.76	+/- 0.36
Si	0.53	+/- 0.05	0.54	+/- 0.05
Cr	0.13	+/- 0.05	0.07	+/- 0.03
Mn	0.04	+/- 0.06	0.02	+/- 0.03
Fe	1.05	+/- 0.08	0.54	+/- 0.04
Cu	3.92	+/- 0.29	1.78	+/- 0.13
Zn	6.96	+/- 0.24	3.07	+/- 0.10
Total	100.00		100.00	

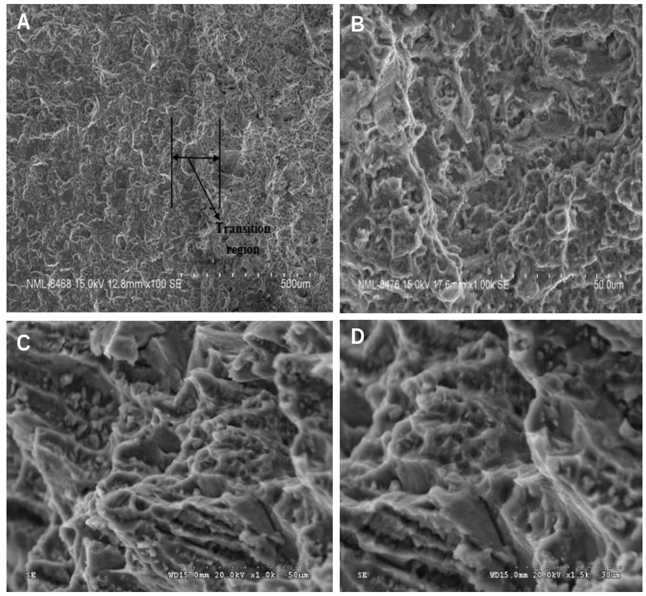

Fig. 10. SEM image of fracture surface of 70% CR 7075 Al alloy; (A) Transition region (fracture precrak and fracture), (B) Fracture surface, (C) Fracture surface (refion-II). (D) Region-II at higher magnification.

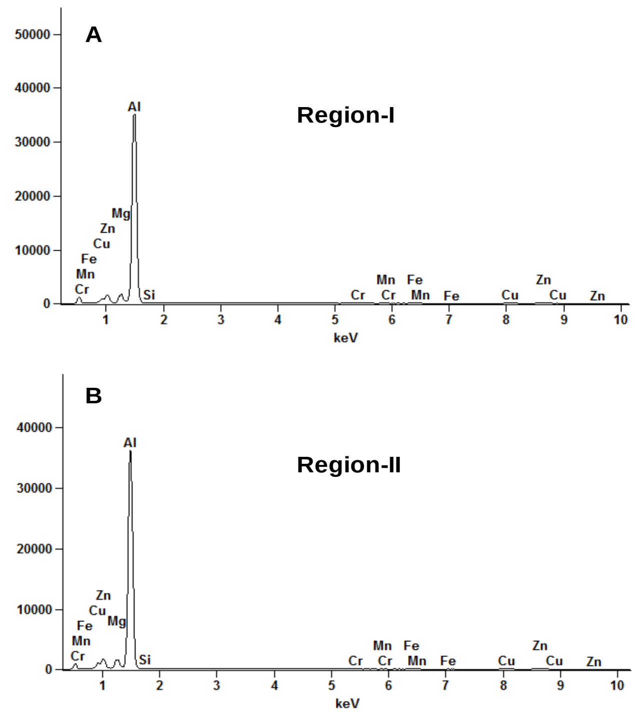

Fig. 11. EDX results at two different regions over the fracture surface of the 70% CR 7075 Al alloy.

The severe strain associated with cryorolling aids to form finer precipitates. Finer precipitates have been observed in case of cryorolled samples (**Fig. 10**) compared to that of bulk alloy (**Fig. 7**). **Fig. 10, 11, 12** and **13** shows the SEM, EDX, X-ray mapping and spot analysis of the elements in case of UFG alloy. Elemental compositions obtained from EDX, in case of UFG alloy, are shown in **Table 3** and **Table 4**.

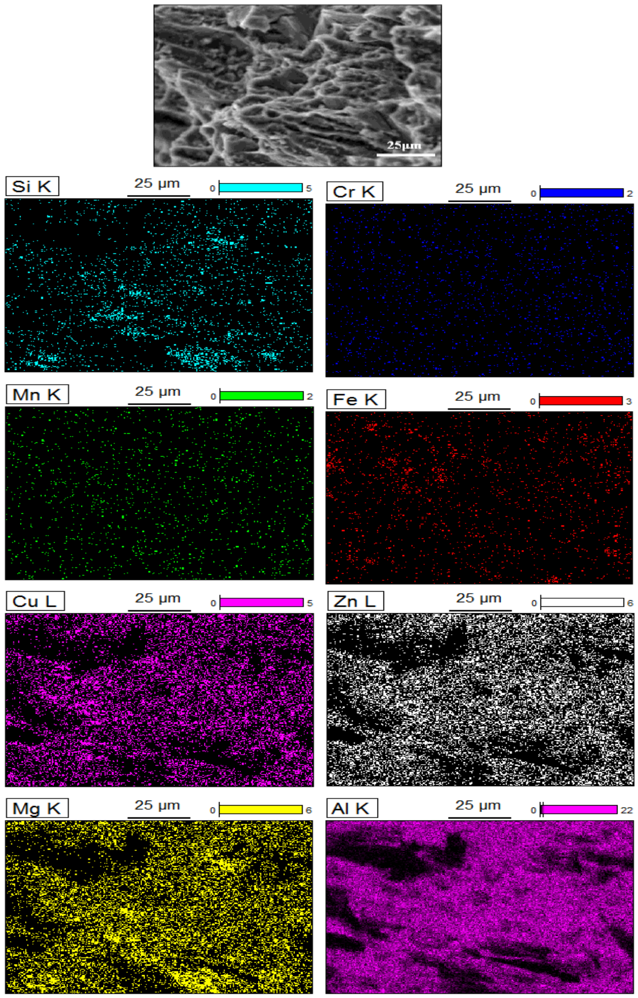

Fig. 12. X-ray mapping of the fracture surface of the 70% CR 7075 Al alloy.

Table 4. EDX composition results at region- II of the UFG alloy fracture surface.

Element	Weight %	Weight % (Error)	Atom %	Atom % (Error)
Mg	3.31	+/- 0.08	3.96	+/- 0.10
Al	83.28	+/- 0.33	89.71	+/- 0.36
Si	0.36	+/- 0.04	0.38	+/- 0.04
Cr	0.25	+/- 0.05	0.14	+/- 0.03
Mn	0.08	+/- 0.07	0.04	+/- 0.03
Fe	0.85	+/- 0.14	0.44	+/- 0.07
Cu	4.61	+/- 0.29	2.11	+/- 0.13
Zn	7.25	+/- 0.38	3.22	+/- 0.17
Total	100.00		100.00	

Presence of coarser precipitates in case of bulk alloy is confirmed from the EDX results, shown in **Fig. 9**. Higher % of Mg and Zn present at the fracture surface points towards the presence of coarser $MgZn_2$ precipitates. Whereas, **Fig. 11** and **Fig. 13** shows lesser amount of Mg and Zn which is attributed to finer precipitates originated from severe strain in case of UFG alloy. XRD study performed in our earlier work also confirms the findings written above **[8]**. Figure 8 in case of bulk alloy and **Fig. 12** in case of UFG alloy shows the uniform distribution of all the alloying elements within matrix of the fractured samples under investigation. The uniform distribution of alloying elements nullifies the possibility of plastic instability in fracture, happens sometimes due to local accumulation of a particular alloying element.

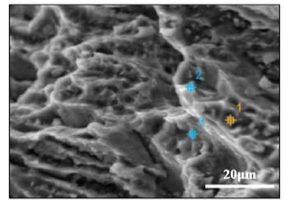

	Mg	Al	Si	Cr	Mn	Fe	Cu	Zn
Point 1	10.90	59.08	0.00	0.08	0.04	0.07	26.11	3.60
Point 2	3.50	88.34	0.00	0.16	0.05	0.12	2.30	5.53
Point 3	2.33	88.07	0.00	0.27	0.07	0.05	1.71	7.50

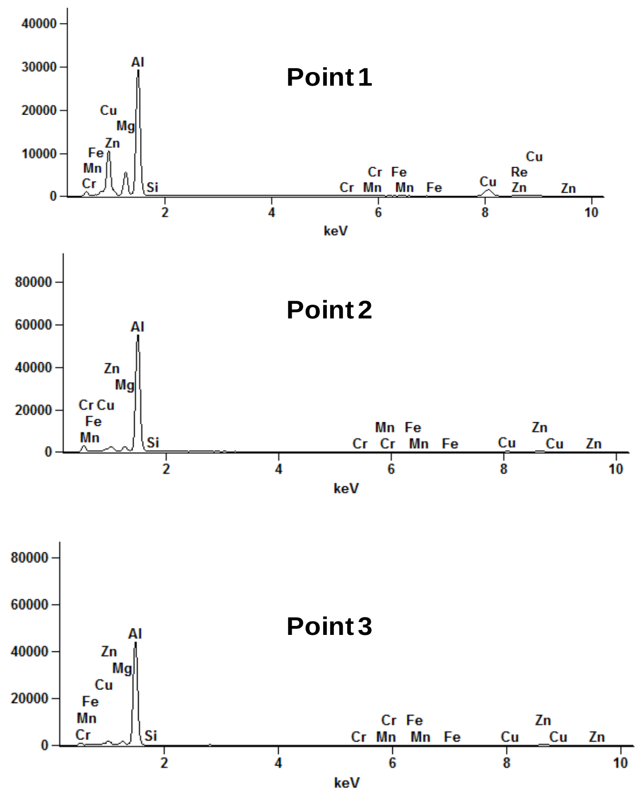

Fig. 13. Point analysis (at three different points) over the fracture surface of the 70% CR 7075 Al alloy.

The average dimple size of the starting materials is 10μm and then it gradually decreases with increasing percentage of thickness reduction attained due to cryorolling (**Fig. 7** and **Fig. 10**). The dimple size gets reduced to less than 1μm after 70% thickness reduction in the cryorolled samples (**Fig. 10**), may be due to the grain refinement and work hardening [**26, 27**], which embarks the significant improvement in fracture behaviour and crack arrest capabilities of the UFG alloy compared to its starting bulk form.

FEM analysis

J integral

In order to determine an energy quantity that describes the elastic-plastic behaviour of tough materials, Rice **[28]** introduced a contour integral, encloses the crack front shown in **Fig. 14**. J integral can be numerically expressed as **[24]**,

$$J = \int_{\Gamma} (w dy - \vec{T} \frac{\partial \vec{\mu}}{\partial x} ds) \qquad (10)$$

Where, J = effective energy release rate (Mpa.m or MN/m). W = Elastic strain energy density or plastic loading work (j/m^3), $\vec{\mu}$ = displacement vector at ds, ds = differential element along the contour, n = outward unit normal to Γ (There is no 'n' in the equation 1).

$\vec{T} \dfrac{\partial \vec{\mu}}{\partial x} ds$ = input work, **s** = arc length, $\vec{T}$ = tension vector (traction forces) on the body bounded by Γ, Γ = arbitrary counterclockwise contour, *J* integral also can be defined as the change in potential energy, *U,* for a virtual crack extension, *da*.

$$J = -\frac{U}{da} \qquad (11)$$

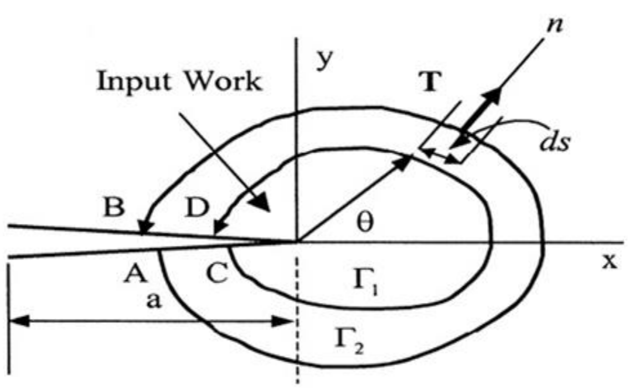

Fig. 14. J-contour integral around the crack surfaces [**13**].

FEM simulation

Assuming elastic-plastic material properties of both UFG and bulk 7075 Al-alloy, FEM simulation of fracture behaviour has been performed in the present work using ABAQUS software using deformation plasticity theory. The domain has been discretized using sweep meshing technique. In sweep meshing technique, an existing volume is meshed by sweeping an area mesh. In this technique, volume mesh can be easily created using brick elements or a combination of brick and prism elements. In this approach, the transition pyramids are automatically generated. Incremental crack growth simulations are performed to show the superior fracture properties of UFG alloy as compared to its bulk form. Whenever a crack growth takes place, it requires some amount of energy to grow.

The computation of *J* integral, stress distribution ahead of the crack tip **[29]** and scaling effect over *J* integral for different crack size, specimen geometry **[30]** have been carried out to understand the improved fracture properties of UFG 7075 Al alloy as compared to its bulk Al alloy.

Table 5. Experimentally evaluated material properties of the 7075 Al alloy under investigation.

Material	E(GPa)		(MPa)	*n*
Al 7075 alloy (Bulk)	72	0.33	260	10
Al 7075 alloy (70% Cryorolled)	72	0.33	540	12
Al 7075 alloy (90% Cryorolled)	72	0.33	610	13

Table 5 shows the difference between elastic–plastic material properties of the 7075 Al alloy in its ultrafine grained form (for 70% and 90% thickness reductions) compared to the bulk alloy, which is obtained after processing the starting bulk alloy by cryorolling technique.

FEM simulations of crack problems have been carried out under quasi-static Mode-I loading using the deformation plasticity theory based on Ramberg-Osgood relationship **[8, 11, 14]**. Stress and strain involving plastic deformation have the following relationship,

$$E.\varepsilon = \sigma + \alpha (\frac{|\sigma|}{\sigma_0})^{n-1} \sigma \qquad (12)$$

Where, σ is the applied stress, σ_o is the yield stress of the material, ε is the strain, E is Young's modulus, α is the "yield" offset, and n (>1) is the hardening exponent (non-linear term) for the plastic deformation. The model is often used to obtain elastic-plastic solutions for fracture mechanics problems where *J* integral is important. For evaluating *J* integral, required strain energy density is computed in this model as,

$$W = \int \sigma \, d\varepsilon \qquad (13)$$

Since this material model is nonlinear, the method followed for stress solutions is described below.

Considering q = ± σ , eq^n (12) solved for σ using Newton's method. Writing C_σ as the correction to σ, the Newton equations for Equation 12 are,

$$\left[1 + n\alpha \left(\frac{q}{\sigma_o}\right)^{n-1}\right] c_\sigma = E\varepsilon - \sigma - \alpha \left(\frac{q}{\sigma_o}\right)^{n-1} \sigma \qquad (13)$$

$$\sigma = \sigma + c_\sigma \qquad (14)$$

Using an initial guess of $\sigma = E\varepsilon$ if, $E\varepsilon \le \sigma_o$ and $\sigma = \pm \left(E\varepsilon\sigma_o^{\,n-1} / \alpha\right)^{1/n}$ (with the sign chosen as the same sign as ε) if $E\varepsilon > \sigma_o$.

In this case, the material stiffness matrix is given by

$$\frac{\partial \sigma}{\partial \varepsilon} = \frac{E}{1 + n\sigma(q/\sigma_o)^{n-1}} \tag{15}$$

Case 1: Edge crack in tension

In the first example, an edge-cracked plate is modeled under pure mode-I loading. **Fig. 15** shows the geometry of an edge cracked plate with height (h=80mm), width (W=40 mm), thickness (B=10 mm) and crack length (a =5mm). The applied value of uniaxial tensile stress (σ) is 200 MPa. Edge crack has been modeled by quadratic reduced integration plain strain elements (CPE8R) following sweep meshing technique. 10 contours were taken to find out exact J integral values for different crack and specimen geometries. **Fig. 16** shows simulations of stress-strain state, plastic dissipation near the crack tip for initial crack length. These key parameters are used to assess the fracture properties of structural components. The present work has been focused on the elastic-plastic ductile fracture behaviour of bulk 7075 Al alloy and its UFG form.

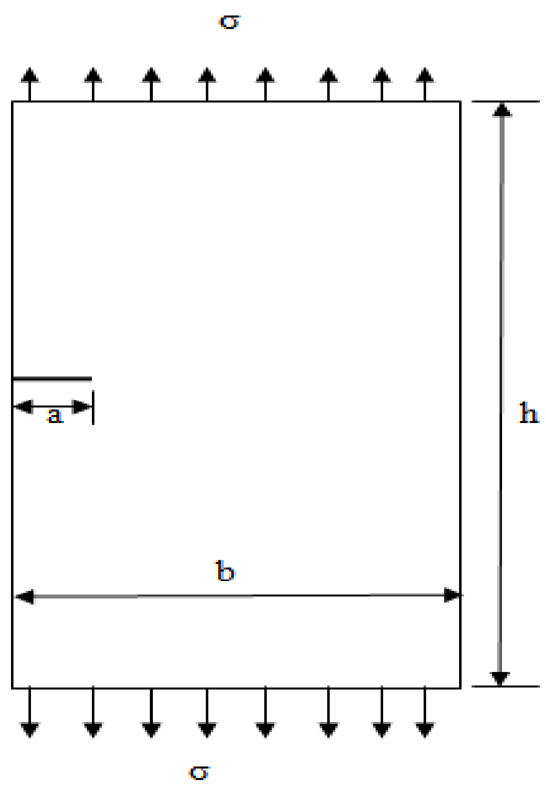

Fig. 15. Edge crack under uniaxial tension.

Fig. 16 (A) shows the Von-mises stress distribution over the cracked plate for both UFG and bulk alloy, respectively. The plastic dissipation ahead of the crack tip and total plastic deformation of the model (**Fig. 16(B)**) is less in case of UFG form of the Al-alloy in comparison to its bulk form due to work hardening effect attained by cryorolling process. Moreover, the UFG alloy shows a higher value of hardening exponent.

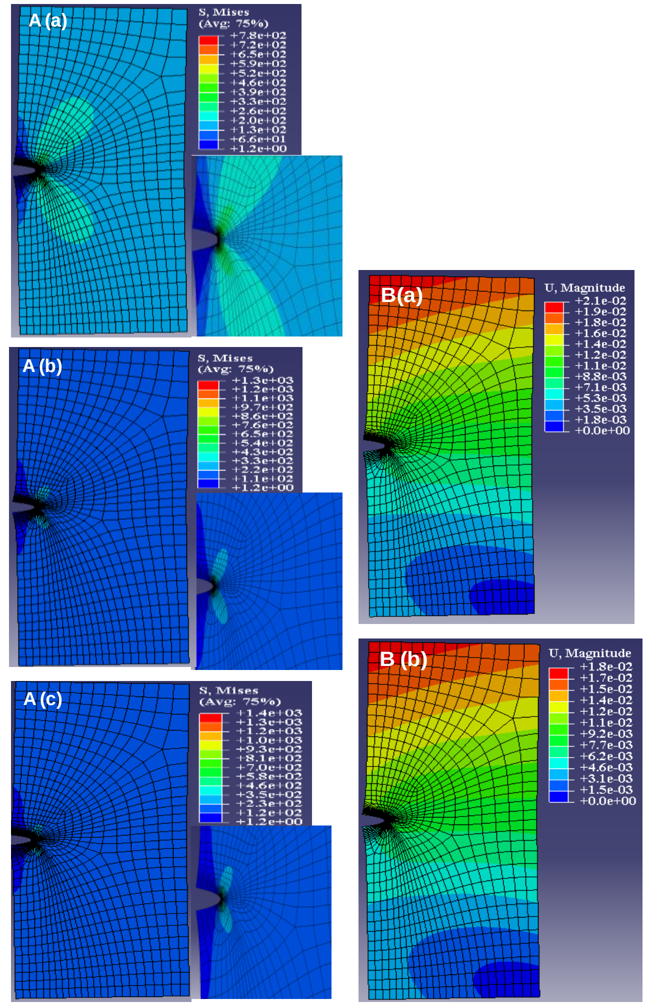

Fig. 16. (A) Von mises stress; (a) Bulk 7075 Al alloy, (b) Ufg (70%) 7075 Al alloy, (c) Ufg (90%) 7075 Al alloy (Zoomed view at the crack tip). (B) Total deformation of the edge cracked plate; (a) Bulk, (b) Ufg (90%).

Fig. 17 presents numerical results for an edge-crack problem. **Fig. 17(a)** shows the J integral values for bulk and UFG alloys (70% and 90% reduced). Decreasing trend in the J values in case of UFG alloys signifies higher load requirement for crack growth under same geometric and loading conditions. Decreasing J values can be explained by higher yield strength of the UFG alloys which hinders the onset of plasticity. This result is also supported by experimental observation of enhanced initiation fracture toughness (J_1), which collectively explains improved crack arrest capabilities of the cryorolled alloy. **Fig. 17 (b)** presents the stress values along crack path for initial crack length of 5 mm, which signifies higher stress values in the vicinity of crack tip for both alloys. **Fig. 17** (**c** & **d**) shows plots of J versus a/W and J versus W/B respectively. These results are obtained by incremental crack growth technique. Plots shown in **Fig. 17** (**c** & **d**) signify crack and specimen size effects over J integral under same loading and geometric conditions of the specimen. Similar trend is observed for both form of the alloy but considerably lower J values obtained in case of UFG alloy with increasing thickness reduction obtained in cryorolling.

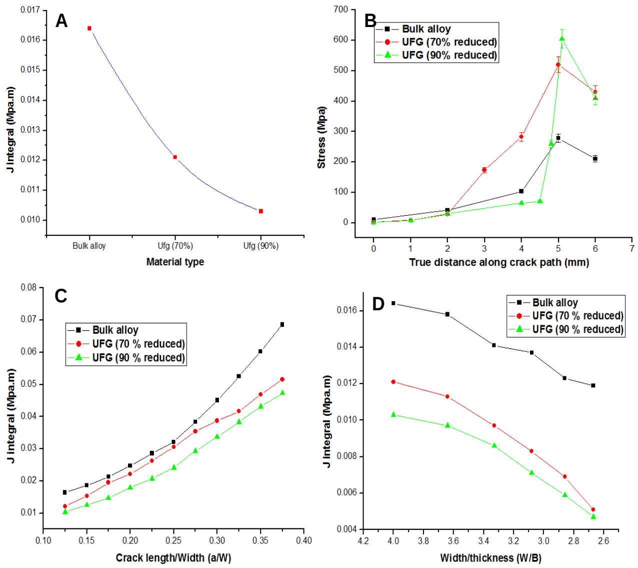

Fig. 17. (a) comparative plot of *J*-integral values, (b) stress values along the crack path, (c) *J* vs. a/W and (d) *J* vs. W/B for all three materials.

Case 2: Centre crack in tension

Fig. 18 shows the geometry of the centre cracked plate having height, h = 80 mm, width, b = 40 mm, thickness, t = 10 mm and crack length, a = 6 mm. The value of uniaxial tensile stress (σ) is 500 MPa. Similar to edge crack problem, current problem also has been modelled by reduced integration plain strain elements (CPE8R) following sweep meshing technique. Von-mises stress distribution over the centre cracked plate for starting bulk and UFG alloys is shown in **Fig. 19**. **Fig. 20** shows the numerical results for the centre-cracked plate under consideration.

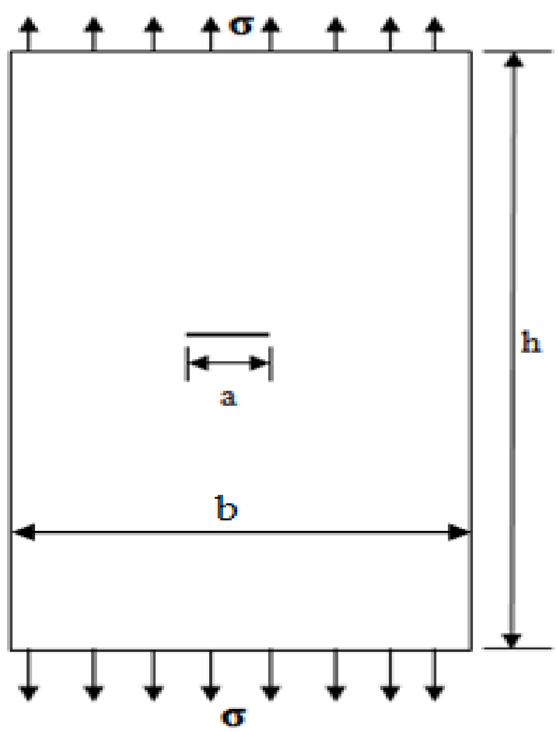

Fig. 18. Center crack under uniaxial tension.

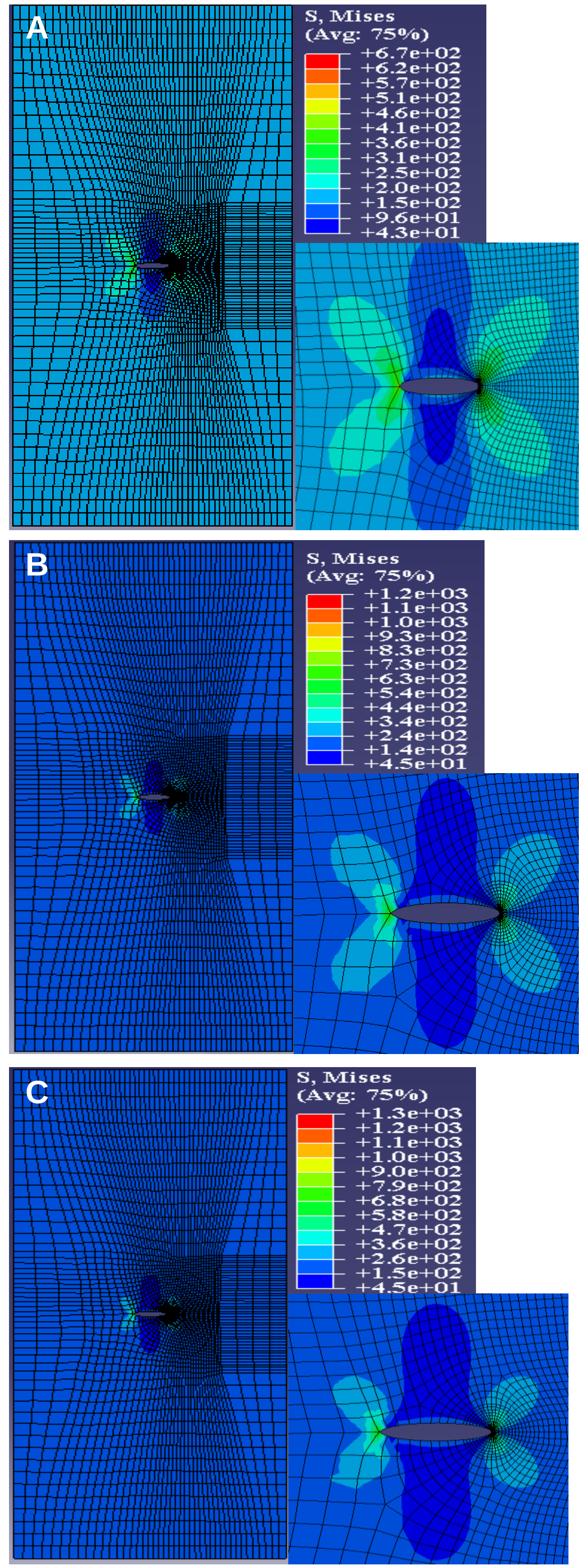

Fig. 19. Von mises stress distribution around crack tip (Zoomed view); (A) Bulk 7075 Al alloy, (B) Ufg (70%) 7075 Al alloy, (C) Ufg (90%) 7075 Al alloy.

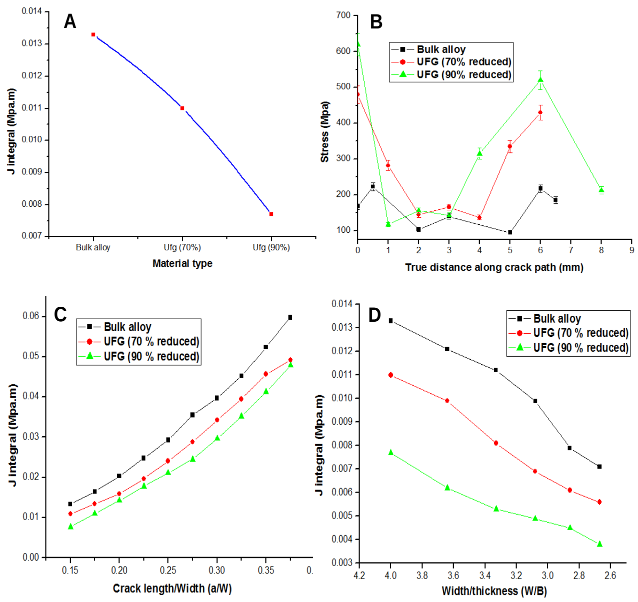

Fig. 20. (a) comparative plot of J integral values, (b) stress values along the crack path, (c) J vs. a/W and (d) J vs. W/B for all three materials.

The results obtained for bulk 7075 Al alloy and its UFG form are compared against each other to show the improved fracture behaviour of the ultrafine-grained alloy. Simulation results confirm improved crack arrest capabilities of the UFG alloy.

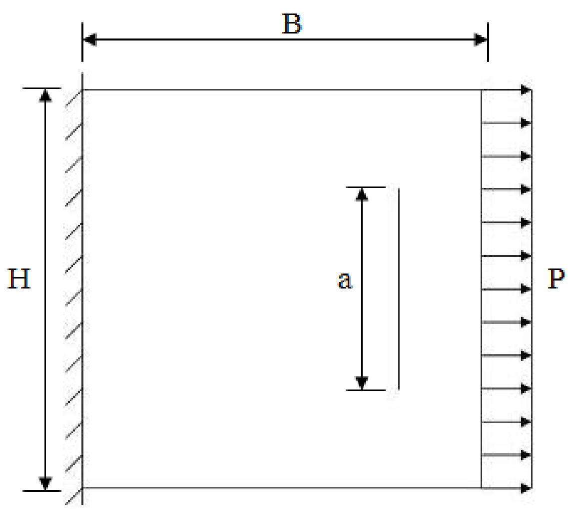

Fig. 21. Cracked plate with Temperature distribution.

Case 3: Temperature assisted crack growth in a plate

Fig. 21 shows the geometry of the cracked plate with combined thermo-mechanical loading having height (H=40mm), width (B=40 mm), thickness (t=10 mm) and through thickness crack length parallel to the right edge is (a=10mm). The value of applied uniform pressure (P) is 100 MPa, applied temperature difference (ΔT) in the plate is 55 ^{0}C and coefficient of thermal expansion is 25.2E-6 /^{0}C. Parabolic temperature distribution has been applied over the total domain of the cracked plate. Initial and final temperature has been considered as 100^{0}c and 155^{0}c. No temperature dependent properties have been used in the present simulations.

Basically, crack growth simulations under thermo-mechanical loading has been performed to show the effect of temperature field on UFG material's flow resistance and crack arrest capabilities. Quadratic reduced integration plain strain elements (CPE8R) are assigned to all regions of the plate. Quad element shape was assigned using medial axis algorithm.

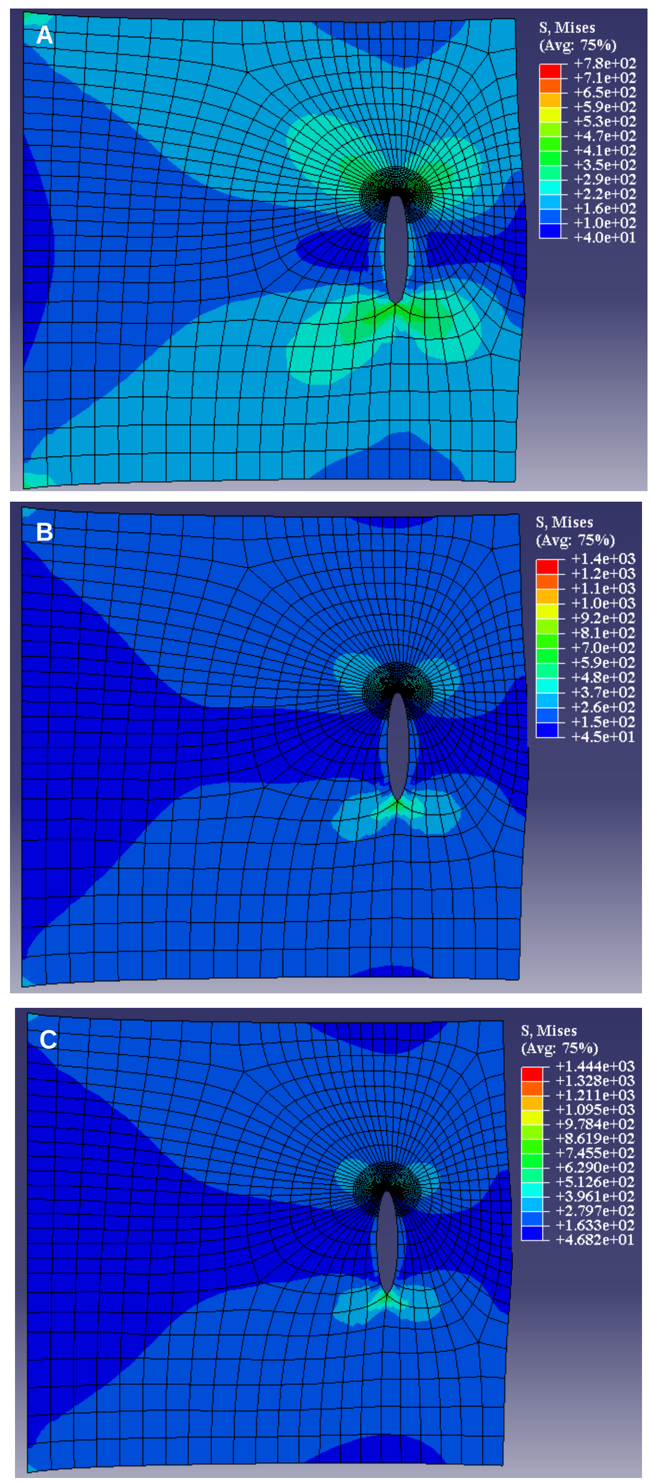

Fig. 22. Von mises stress distribution in the cracked plate.

In this example along with mechanical loading in the form of uniform pressure, temperature distribution is applied in the cracked plate. Application of temperature field makes plastic deformation easier and higher *J* values are observed compared to other case studies for both bulk and UFG alloy. **Fig. 22** shows the von-mises stress distributions along with temperature distribution in the cracked plate. **Fig. 23** (**a,b,c** & **d**) presents *J* integral for bulk and UFG alloys, stress values along crack path and variation of *J* with crack and specimen size. Highest Stress values at the crack tip can be seen for all three materials. *J* integral values get decreased with the increasing cryorolling thickness reductions due to enhanced hardening exponent. It explains better crack arrest capabilities of the UFG alloys due to higher load requirement to reach plasticity regime. So, thermo-mechanical loading aids to improve the crack arrest capabilities of UFG alloys.

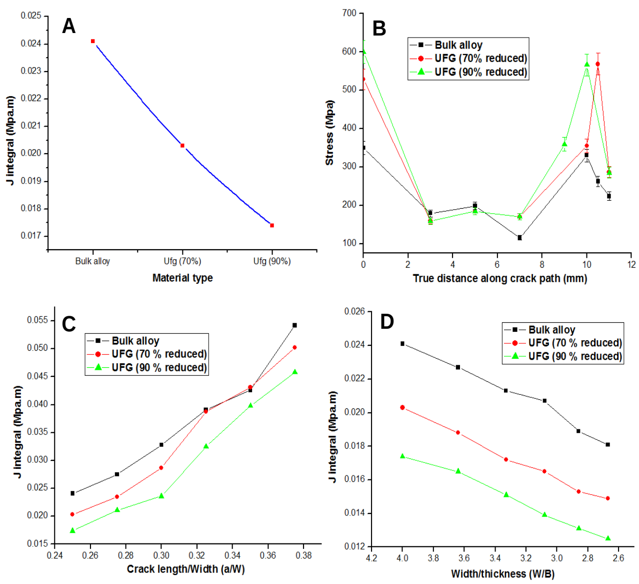

Fig. 23. (a) Comparative plot of *J* integral values, (b) stress values along the crack path, (c) *J* vs. a/W and (d) J vs. W/B for all three materials.

Conclusion

In the present work, bulk Al 7075 alloy has been cryorolled to produce ultrafine-grained Al alloy. Microstructural characterizations have been carried out by using optical microscopy, FESEM and TEM for bulk and UFG alloys, respectively. Mechanical characterizations have been performed by using hardness testing, tensile testing to demonstrate improved properties of the bulk alloy in its UFG form. Initiation fracture toughness determined using compact tension specimens has shown the improved crack arrest capabilities of the UFG 7075 Al alloy. Cryorolling made significant improvement in the mechanical properties of the alloy under consideration compared to room temperature rolled alloy, due to hindrance of dynamic recovery and grain growth. Grain refinement enhances initiation fracture toughness of the UFG alloys which hinders onset of plasticity and improves crack growth resistance. Fracture surfaces also show evidence of grain refinement with the increasing cryorolling thickness reduction. Experimental observations of improved fracture properties of cryorolled alloys are validated using FEM simulations. Elastic-plastic material properties such as yield strength, hardening exponent were measured by tensile test, and used as input for FEM simulations. Three case studies are selected to show improved crack arrest capabilities of the UFG alloys (70% and 90% reduced). These simulations show a higher load requirement for same boundary and geometric conditions in case of UFG Al alloys (70% and 90% reduced) for unstable crack extension. A comparative analysis between bulk and UFG alloys has shown a decreasing trend in *J* integral for UFG alloys due to enhanced hardening exponent. A higher load requirement in case of cryorolled Al alloy to reach *J* integral to J_1 (evaluated experimentally), establish its improved crack arrest capability due to the effective grain refinement in the ultrafine grain regime.

Acknowledgements

The author, Mr. Prosenjit Das, would like to thank Prof. Gautam Biswas, Director, CSIR-CMERI, for his support and encouragement to this work. The author, Dr. R. Jayaganthan, would like to thank DST, New Delhi for their financial support to this work through grant no: DST-462-MMD.

Reference

1. Wang Y.; Chen M.; Zhou F.; Ma E. *Nature*. 2002, 419, 912.
   DOI: 10.1038/nature01133
2. Lee T.R.; Chang C.P.; Kao P.W. *Mater. Sci. Eng. A*. 2005, 408, 131.
   DOI: 10.1016/j.msea.2005.07.045
3. Panigrahi S.K.; Jayaganthan R. *Mater. Sci. Forum*. 2008, 584–586, 734.
   DOI: 10.4028/www.scientific.net/MSF.584-586.734
4. Rangaraju N.; Raghuram T.; Krishna B.V.; Rao K.P.; Venugopal P. *Mater Sci. Eng. A*. 2005, 398, 246.
   DOI: 10.1016/j.msea.2005.03.026
5. 5. Lee Y.B.; Shin D.H.; Park K.T.; Nam W.J. *Scripta Mater*. 2004, 51, 355.
   DOI: 10.1016/j.scriptamat.2004.02.037
6. Shanmugasundaram T.; Murty B.S.; Sarma V.S. *Scripta Mater*. 2006, 54, 2013.
   DOI: 10.1016/j.scriptamat.2006.03.012
7. Jayaganthan R.; Panigrahi S.K. *Mater. Sci. Forum*. 2008, 584– 586, 911.
   DOI: 10.4028/www.scientific.net/MSF.584-586.911
8. Das P.; Jayaganthan R.; Chowdhury T.; Singh I.V. *Mater. Sci. Eng. A*. 2011, 528, 7124.
   DOI: 10.1016/j.msea.2011.05.021
9. Das P.; Jayaganthan R.; Chowdhury T.; Singh I.V. *Mater. Sci. Forum*. 2011, 683, 81.
   DOI: 10.4028/www.scientific.net/MSF.683.81
10. Tiwari A.; Mishra A. K.; Kobayashi H.; Turner A. P. F. *Intelligent Nanomaterials",* Wiley-Scrivener Publishing, USA,
    ISBN: 978-04-709387-99, 2012.
11. Yang Z. Mech. Res. Commun. 2005, 32, 514.
    DOI: 10.1016/j.mechrescom.2004.10.001
12. Fan C.; Ben Jar P.Y.; Roger Cheng J.J. *Eng. Fract. Mech*. 2007, 74, 1243.
    DOI: 10.1016/j.engfracmech.2006.07.014
13. Sukumar N.; Prevost J.H. *Int. J. Solids Struct.* 2003, 40, 7513.
    DOI: 10.1016/j.ijsolstr.2003.08.002
14. ABAQUS Analysis User's Manual (Version 6.9), United States of America, ABAQUS Inc., 2009
15. Das P.; Singh I.V.; Jayaganthan R. *Journal of Materials Engineering and Performance*. 2012, 21, 1167.
    DOI: 10.1007/s11665-011-0062-6
16. Das P.; Jayaganthan R.; Singh I.V. *Mater. Des.* 2011, 32, 1298.
    DOI: 10.1016/j.matdes.2010.09.026
17. Das P.; Singh I.V.; Jayaganthan R. *Int. J. of Materials and Product Technology*. 2012, 44(3/4), 252.
    DOI: 10.1504/IJMPT.2012.050192

18. ASTM Standard E8/E8M, 2009, ''Standard Test Methods for Tension Testing of Metallic Materials,'' ASTM International, West Conshohocken PA, 2009.
DOI: 10.1520/E0008-E0008M-09, www.astm.org
19. ASTM Standard E647, 2008, ''Standard test method for measurement of fatigue crack growth rates,'' Annual Book of ASTM Standards, 2008.
20. ASTM Standard E1820-09e1, ''Standard Test Method for Measurement of Fracture Toughness,'' ASTM International, West Conshohocken PA, 2009.
DOI: 10.1520/E1820-09E01, www.astm.org
21. Gupta S.K.; Bhasin V.; Vaze K.K.; Ghosh A.K.; Kushwaha H.S.; Chapuliot S.; Marie S.; Kayser I. *International Journal of Pressure Vessels and Piping*. 2006, 83, 686.
DOI: 10.1016/j.ijpvp.2006.05.004
22. Margolin B. Z.; Kostylev V. I.; Minkin A. I. *Strength of Materials*. 2002, 34, 120.
23. Valiev R. Z.; Islamgaliev R. K.; Alexandrov I.V. *Prog. Mater. Sci*. 2000, 45, 103.
PII: S0079 - 6425(99)00007-9
24. Perez N. Fracture Mechanics, Kluwer Academic Publishers, U.S.A, 2004, p. 135-140.
25. Gariboldi E.; Ripamonti D.; Signorelli L.; Vimercati G.; Casaro F. *Metallurgical Science and Technology*. 2007, 25, 3.
26. Panigrah S.K., Jayaganthan R. *Mater.Sci. A.* 2008, 480, 299.
DOI: 10.1016/j.msea.2008.03.029
27. Wang Z.C; Prangnell P.B. *Mater Sci. Engg. A*. 2002, 328, 87.
DOI: 10.1016/S0921-5093(01)01681-1
28. Rice J.R. *J. Appl. Mech*. 1968, 35, 379.
DOI: 10.1115/1.3173668
29. Chattopadhyay J.; Tomar A.K.S.; Dutta B.K.; Kushwaha H.S. *Engineering Fracture Mechanics*. 2005, 72, 2186.
DOI: 10.1007/s10704-007-9166-2
30. Lu C.; Danzer R.; Fischer F. D. *Journal of the European Ceramic Society*. 2004, 24, 3643.
DOI: 10.1007/s10704-007-9166-2